2.15 MODELING THE EFFECT OF IODIDE DISTRIBUTION ON OZONE DEPOSITION TO SEAWATER SURFACE

In-Bo Oh[a], Daewon W. Byun[a,*], Hyun-Cheol Kim[a], Soontae Kim[a], Bob Cameron[b]

[a]Institute for Multi-dimensional Air Quality Studies, University of Houston, Houston, TX
[b]Gulf of Mexico OCS Region, Minerals Management Service, New Orleans, LA

1. INTRODUCTION

Deposition to the seawater surface can be an important removal pathway for the atmospheric ozone. Because of its potential for affecting the ozone budget and lifetime in the marine boundary layer and influencing onshore/inland distribution of ozone, proper treatment of the ozone deposition over the coastal area is needed to improve coastal ozone estimates by the regional air-quality models. Large differences in the observed deposition velocities are reported in the literature with values ranging from 0.01 to 0.12 cm s^{-1} for sea water (Gallagher et al., 2001; Kawa and Rearson, 1989; Lenschow et al., 1982; Galbally and Roy, 1980). This wide range of deposition velocities can differently affect ozone loss in marine air.

Ozone deposition into seawater is dominantly determined by the surface uptake efficiency that is controlled by complicated physical and chemical processes (Lenschow et al, 1982). In particular, the chemical loss by uptake of the dissolved iodide reacting with ozone is an important deposition mechanism for ozone over the sea. Garland et al. (1980) suggest that dissolved iodide make a substantial contribution to the deposition of ozone to seawater. More recently, Chang et al.(2004) confirmed the finding of Garland et al. (1980) and identified iodide as the only specie capable of significantly enhancing ozone deposition.

In this study, we extend the approach of Chang et al. (2004) to the CMAQ modelling system by incorporating reasonable iodide concentrations estimated from satellite measurements over the Gulf of Mexico and assess the effects of iodide distribution on ozone deposition onto the seawater surface. Here we also present some results of the spatiotemporal changes in the ozone deposition and ambient ozone concentration patterns by the iodide effects for a marked sea breeze day

2. MODIFICATION OF OZONE DEPOSITION MODULES IN CMAQ

We utilized the Model-3/CMAQ dry deposition (M3DDEP) module in MCIP (version 3.0) linked to MM5 with land-surface model to calculate ozone deposition velocity. When estimating deposition to open water, only water surface resistance (r_{gw}) needs to be considered in the surface resistance term (R_c). Thus, R_c is replaced by the r_{gw} according to Slinn et al. (1978); r_{gw} describes both chemical reactions and physical transport across the air-sea interface, which is similar structure to that of Liss and Merlivat (1986). However, the parameters needed for calculating surface resistance over the seawater are quite uncertain for ozone. Moreover, the current formulation cannot account for ozone deposition taking place without wind, though substantial ozone deposition may occur by chemical reactions (mainly iodide reactions) at low wind speeds (Gabally and Roy, 1980).

In order to consider ozone loss by a chemical reaction ($O_3 + I^-$) in the seawater microsublayer, the original water surface resistance parameterization in the M3DDEP module of the CMAQ system was replaced with the equation proposed by Chang et al. (2004), which accounts for the ozone deposition to the sea surface due to the iodide reaction, combining Garland's (1980) and Liss and Merlivat's (1986) formulations:

$$r_{gw} = \frac{H}{a k_w + \sqrt{\lambda D}} = \frac{1}{p k_w + q}, \quad \lambda = \sum_i k_i C_i \qquad (1)$$

where H is the dimensionless Henry's law constant, and k_w is gas-transfer velocity as a function of wind speed. The a term is a chemical enhancement factor, λ and D denote the integrated chemical loss of ozone by the species i (e.g., iodide, dimethylsulfide, and alkenes) and the molecular diffusivity of ozone in water, respectively. For λ term, k_i and C_i are a second order kinetic rate and observed surface concentration (C_i) of a species i. In this study, the k_w term was derived from the formula of Wanninkhof (1992) and the averaged p value of 1.75 was obtained from the linear regression analysis of Chang et al. (2004) utilizing a large set of observational open-sea data of Kawa and Pearson (1989) (see Fig 3). In order to determine the q value, iodide concentrations from satellite-derived estimates of near-surface chlorophyll concentration were utilized together with dimethylsulfide (DMS) and alkenes concentrations as suggested by Kettle et al. (1999) and Riemer et al. (2000), respectively (see Table 1 of Chang et al., 2004). The M3DDEP module was changed, including the related I/O modules and the MCIP processor run was performed to calculate dry deposition velocities of ozone.

* *Corresponding author address*: Daewon W. Byun, Univ. of Houston, Houston, TX; Tel.: + 1 713 743 0707; fax: + 1 713 743 0604; e-mail: dbyun@mail.uh.edu

3. MODEL CONFIGURATIONS AND BASE CASE SIMULATIONS RESULTS

One-month period (July 21 to August 20) in 2005, which does not include days affected by either the hurricane Emily or Katrina, was selected for the MM5 and CMAQ simulation to quantitatively assess the iodide effects on the dry deposition of ozone in the Gulf of Mexico. The selected period may be appropriated for identifying the influence of chemical processes of iodide on the ozone dry deposition to seawater as well as ambient concentrations in the coastal area because of the prevailing light winds over the sea and frequent land-sea breeze circulations observed in the Gulf Coast.

Modeling domain: The horizontal modeling domain structure consists of nested grids of varying resolution: a coarse grid domain (36-km cell size, 133 × 91 array) that covers the conterminous United States and a regional domain (12-km cell size, 167 × 128 array) over the southern States neighboring the Gulf of Mexico. Both MM5 and CMAQ modeling domains are defined on a Lambert Conformal mapping projection, following the perfect sphere definition used in MM5 The horizontal grids employed for the CMAQ modeling are subsets of the grids used in MM5. The coverage of the MM5 and CMAQ 36- and 12-km regional grid are shown in Fig. 1.

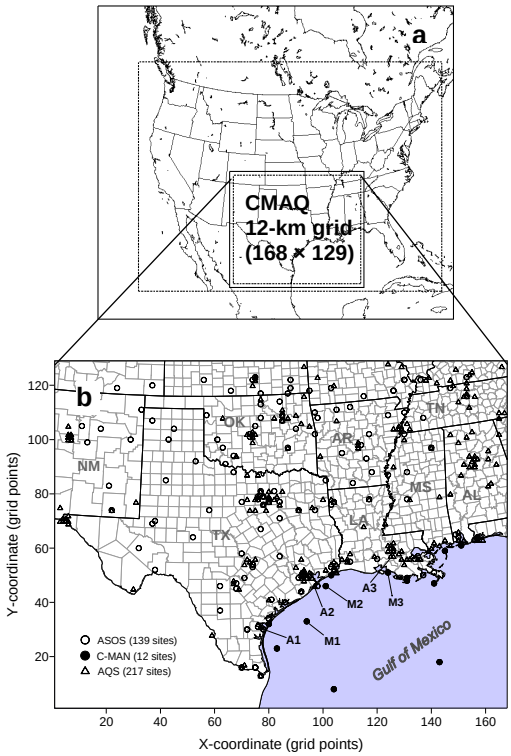

Fig. 1. (a) Map showing Lambert 36 and 12-km grid nests used for MM5-CMAQ modeling. (b) The locations of observations used for model verification. Selected meteorological and ozone monitoring sites denoted by M1-3 and A1-3, respectively (M1: Freeport (buoy), M2: Galveston (buoy), M3: Salt Point (shorebased tower), A1: Corpus Christi (residential), A2: Galveston (commercial), A3: Belleview Rd.(agriculture))

Vertical grid structure: There are 43 and 23 vertical sigma layers for MM5 and CMAQ, respectively with higher resolution near the ground to better understand both the atmospheric structure and chemical processes in the lower boundary layer. CMAQ uses 23 layers by collapsing two to three layers in the upper part of the MM5 43 layers. The MM5 and CMAQ vertical layer structures are same for two nested domains.

MM5 modeling: The MM5 (v 3.6.1) model run was performed utilizing the 24-category land use data from USGS and initial/lateral boundary conditions generated by interpolation of the NCEP "ETA" model analysis fields. The explicit moisture scheme for simple ice, the radiation scheme of rapid radiative transfer model (RRTM), and the surface scheme for the Noah land surface model (LSM) were adopted and the planetary boundary layer (PBL) was parameterized using the MRF-PBL. Specifically, grid nudging was performed at 3-hourly intervals both for the two-dimensional surface fields and for the three-dimensional fields aloft.

Emission processing: Model-ready emissions estimates to generate a gridded emission inventory for CMAQ were developed using the Sparse Matrix Operator Kernel Emissions system (SMOKE). The data sets processed with SMOKE were obtained from Texas emission inventory (TEI) of Texas Commission on Environment Quality (TCEQ) (TCEQ, 2004), TEI offshore emissions (platform and non-platform), Minerals Management Service (MMS) 2000 Gulf-Wide Emissions Inventory (GWEI), and 2000 GOADS Non-Platform Area Source Inventory. For meteorological data for biogenic emissions, 10-m temperature and solar radiation estimated from MM5-MCIP were used. The CB-IV chemical mechanism was used for chemical speciation of volatile organic compounds.

CMAQ modeling (MCIP and CCTM): The MCIP (v 3.0) options used in processing the MM5 out fields were: (1) the “pass-through” option where PBL values as estimated by MM5 were used directly; (2) radiation fields from MM5 files were used; and (3) Modified Model-3/CMAQ dry deposition (M3DDEP) routine was utilized to calculate dry deposition velocities.

The CCTM (v 4.5) simulation used the CB-IV gas-phase chemistry mechanism; RADM-type aqueous chemistry and subgrid cloud processes; and the efficient Euler backward iterative (EBI) solver. Advection scheme chosen for the model was the piecewise parabolic method (PPM). The multiscale horizontal diffusion scheme was based on local wind deformation and vertical diffusion was derived from eddy diffusivity theory.

Evaluation for the base case simulation results: In order to establish the accuracy of meteorological and ozone modeling in assessing iodide effects on ozone deposition, we first performed a MM5-CMAQ run for a base case not linked with modified dry deposition model. The MM5 evaluation was performed by comparing the modeled 10-m temperature and winds with the observed ones in a regional 12-km domain during the whole

simulation period. Observed data were collected at 151 sites from the Automated Surface Observing System (ASOS) of National Weather Service (NWS) and Coastal Marine Automated Network (C-MAN) (Fig. 1).

Table 1 presents the statistical summaries of the comparison of the modeled temperature, wind speed and u- and v- wind components with surface observations over the all 151 sites and 12 offshore sites, respectively. Overall, there is good agreement between the modeled and observed values. The modeled temperature agrees well with the observations within 1℃ and has a good correlation (R = 0.9) with observations. The MM5 model also captures well wind speed and u and v components with reasonable accuracy for all statistical measures. For comparison with observations at offshore sites, most statistics (values in parentheses in Table 1) show better agreement between the modeled and observed ones. It is noted that the modeled wind speed at offshore sites (see Fig. 1), that is closely associated with computing k_w in Eq. (1), have a very good agreement with observations, achieving small bias and errors (mean bias, MB = -0.23 and root mean square error, RMSE = 1.25) and high correlation (R = 0.8).

Table 1. MM5 performance statistics for hourly temperature and winds at 151 sites during the entire modeling period. The values in parenthesis indicate statistics for 12 offshore sites

Statistical measures	Temp. (K)	Winds (m s^{-1})		
		WS	U	V
MB	-0.62 (-0.34)	-0.40 (-0.23)	0.63 (0.44)	0.43 (0.79)
RMSE	2.14 (1.10)	1.59 (1.25)	1.93 (1.91)	1.92 (2.02)
R	0.90 (0.65)	0.70 (0.80)	0.62 (0.75)	0.76 (0.77)
No. samples	107850 (8132)	100420 (8062)		

Evaluation for surface ozone was performed by comparing the modeled concentrations with available ground measurements collected at 217 sites of Air Quality System (AQS) of U.S. EPA (see Fig.1). The statistics were calculated in terms of R, RMSE, mean normalized bias error (MNBE) and mean normalized gross error (MNGE) for the entire simulation period. Both MNBE and MNGE were made using observation-simulation pairs (cut-off level of 40 ppb for hourly concentrations). The results showed that there was good agreement with a strong correlation of 0.81 with RMSE of 13.2 ppb and ozone concentrations were successfully simulated with low values of -3.7% and 9.8% for MNBE and MNGE, respectively, which satisfy the recommended criterion of having values not exceeding ±5–15% and 30–35% for the respective statistics.

4. RESULTS AND DISCUSSION

4.1 water surface resistances

Surface resistance (r_{gw}) for ozone uptake to sea water surface was tested for different cases of iodide concentrations and wind velocities. Fig. 2 shows the r_{gw} calculated by Eq. (1) with different iodide concentrations of 100, 200, 300 and 400 nM for wind speeds in the range of 0 – 20 m s^{-1}. The range of r_{gw} values can be comparable to the previous chamber measurements (1390 – 3400 m s^{-1}) reported by Aldaz (1969) and Galbally and Roy (1980), and aircraft data (1690 – 1890 m s^{-1}) obtained by Lenschow et al. (1982). All curves present well the significant dependence of the resistance on surface wind speed, but the wind influences are less with the higher iodide concentrations due to dominant chemical processes. The large differences in surface resistances among four different iodide concentrations under lower wind speed regimes clearly indicate that chemical enhancement induced by iodide reaction gives a rise to reduce the resistances for ozone uptake to sea water surface.

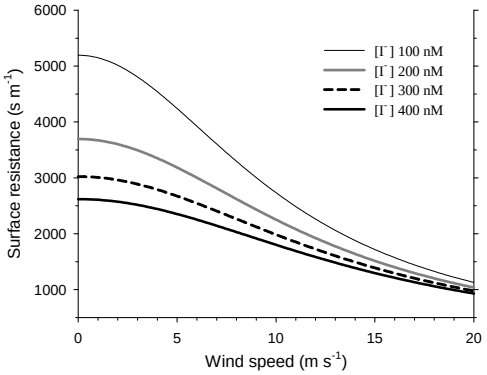

Fig. 2. Surface resistances for ozone uptake $r_{gw[O_3]}$ (s m^{-1}) to the sea surface as a function of 10-m wind speed. Individual curves are corresponding to different iodide concentrations (100, 200, 300 and 400 nM). The dimensionless Henry's law constant was calculated by applying fixed temperature of 288 K.

4.2 ozone dry deposition velocities

In order to evaluate the variability in ozone dry deposition velocities from the modified M3DDEP model and to identify the sensitivity of the model to changes in iodide concentrations, we compared the results from three different modeling cases (Case 1 (base case): original M3DDEP, Case 2: modified M3DDEP without iodide reaction, and Case 3: modified M3DDEP with iodide reaction). Fig. 3 shows the modeled ozone dry deposition velocities for different modeling cases and observations as a function of 10-m wind speed. All curves were generated with the modeled values at the lowest layer for the entire sea area in the 12-km domain. Three curves for Case 3 indicate ozone dry deposition velocities for iodide concentrations of 100, 200-300 and 400 nM, respectively.

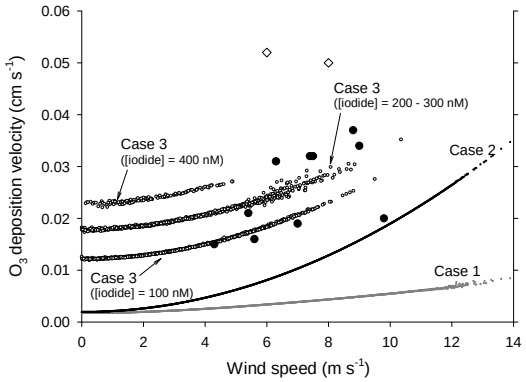

Fig. 3. Dry deposition velocity for ozone as a function of wind speed. The individual curves are for different modules: M3DDEP (Case 1); modified M3DDEP without iodide reaction (Case 2); modified M3DDEP with iodide reaction (Case 3). Two curves for Case 3 indicates deposition velocities corresponding to different iodide concentrations (100 and 400 nM) extracted from model results during August, 2005. The filled circles indicate observations of Kawa and Pearson (1989). Solid squares and a solid diamond indicate observations of Lenschow et al., (1982) over the Gulf of Mexico and the North Pacific, respectively.

Ozone deposition velocities of Kawa and Rearson (1989) and Lenschow et al. (1982), which were measured from aircraft by the eddy correlation technique over the northeast Pacific Ocean and Gulf of Mexico, respectively, are also presented to compare with the model results. Unfortunately, direct comparison with observations for ozone dry deposition velocities and their dependence on iodide concentrations over the northeast Gulf of Mexico are not yet available due to a lack of in-situ measurements. It should be noted that Case 1 shows very low deposition velocities with weak dependence on wind speed compared with those for other cases and observations. The large differences between the curve for Case 1 and the scatter of the observed values indicate that current M3DDEP does not provide reasonable deposition velocities for ozone over the sea for a wide range of wind speed. The deposition velocities for Case 2 show exponential increase with wind speed, but with near zero values occurred at low wind speeds due to the iodide reaction is ignored.

On the other hand, curves for Case 3 clearly exhibit much higher deposition velocity values than those for Case 2, implying that ozone loss by iodide reaction can play a major role in the deposition of ozone in the sea water microsublayer. In particular, the significant increase of the deposition velocity with wind at low wind speeds demonstrates that substantial ozone deposition, i.e., the uptake of ozone by iodide reactions in the microsublayer, does take place. The large set of observational data of Kawa and Rearson (1989) fall well within the range of modeled values between the two curves (for 100 and 400 nM) for Case 3, suggesting that modified model considering iodide concentrations of 100~400 nM can reasonably estimate the observed range for dry deposition velocities for ocean water. The modeled values, however, appears to be somewhat lower than two observations of Lenschow et al. (1982) and several previous estimates for seawater (Gallagher et al., 2001), which may mainly due to large uncertainties in the various sea surface chemical–uptake processes including the concentration field of chlorophyll.

4.3. Iodide effects on ozone dry deposition during one month

Table 2 summarizes one-month average dry deposition velocities and 10-m wind speeds obtained from modeling results for three cases. All data used here were hourly modeled values for the entire sea area in the 12-km domain (167×128 array). The average deposition velocities for Case 1 and 2 are close to each other in spite of the large differences in the dependency on wind speed as shown in Fig. 3 because large regions of the ocean had low wind speeds for a significant fraction of time. On the other hand, deposition velocity for Case 3 differs remarkably from those of Case 1 and 2, by nearly an order of magnitude. The difference is more clearly identified in minimum values for three cases. As expected, Case 3 generated higher deposition velocities for ozone compared to other two cases because the iodide effect combined with wind dependency was properly considered in the modified model. Through the comparison between Case 2 and 3, it is estimated that about 70 % of the enhancement in the ozone dry deposition velocity in Case 3 is attributed to the iodide effect alone.

Table 2. Surface dry deposition velocities for ozone and 10-m wind speed from the different modeling cases. The values were averaged for the entire sea area in a regional domain (12 km cell size) over a period of one month. Note that maximum and minimum values are from those among daily averages.

Case	Dry deposition velocity for ozone (V_d, cm s^{-1})			10-m wind speed (m s^{-1})
	Average ± S.D.	Max.	Min.	
1	0.0026 ± 0.0003	0.0036	0.0022	
2	0.0050 ± 0.0014	0.0092	0.0032	3.77 ± 0.97 Max. = 6.29 Min. = 2.35
3	0.0160 ± 0.0015	0.0210	0.0139	

Significant differences between the deposition velocities for Case 2 and 3 were found mostly near the coast in response to the dramatic changes in estimated iodide concentrations from the shore to the sea (Fig. 4a and b). Marked changes in iodide concentrations near the coast coincide with chlorophyll a distributions as was observed in the southeastern U.S. continental shelf water by Wong and Zhang (1992). It is noted that the largest differences are shown near the coast of New Orleans, Louisiana (LA), which was caused by higher chlorophyll concentrations associated with biological productivity (Rabalais et al., 1993) driven mostly by the nutrient effluents from the Mississippi River. Fig. 4b and

c also indicate that ozone uptake by iodide is a predominant factor determining deposition velocities at low wind speeds.

The increased deposition velocity for Case 3 leads to the enhancement of ozone deposition onto the seawater. Fig. 4d shows the difference in the ozone deposition amounts between Case 2 and 3 during one month, calculated by multiplying the concentration in the lowest model layer with dry deposition velocity. The difference pattern for deposition amounts is quite similar to that for the dry deposition velocities as in Fig. 4b although that is primarily dependent on the ozone concentrations determined by the photochemical and meteorological processes. The total difference, that is accumulated over the one month period for the sea water, was about 932 kg hectare^{-1} (199 g hectare^{-1} on a grid average) which might be small, but it can have significant consequences for the large-scale ozone budget when summed over the entire coastal water areas.

The large differences were found offshore near the shoreline, especially near the coast of New Orleans with the maximum of 424 g hectare^{-1}, corresponding to an area of high iodide concentrations. Conversely, it is interesting to note that negative values were found inland from the shoreline, which is extended much further inland. This indicates that the enhanced ozone deposition velocities over the sea can affect ozone deposition in the inland coastal area as the marine air mass with lower ozone concentration is advected from offshore to the inland under onshore wind conditions.

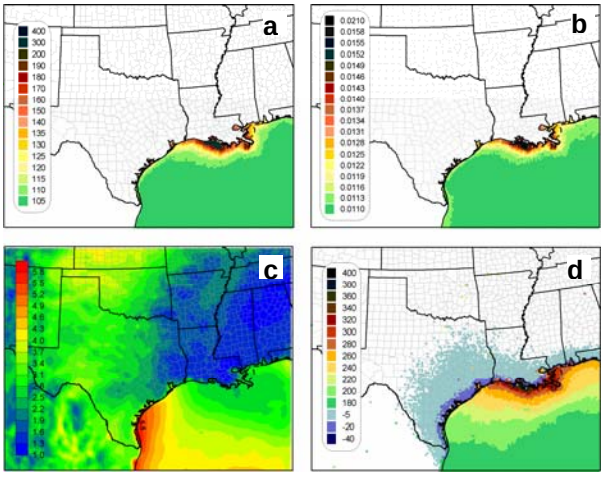

Fig. 4. (a) Estimated iodide concentrations (nanomole L^{-1}, nM) from satellite-derived estimates of near-surface chlorophyll concentrations for a 12-km regional domain, differences between Case 2 and 3 (Case 3 minus 2) in (b) ozone dry deposition velocities (cm s^{-1}), (c) 10-m wind speeds (m s^{-1}) and (d) ozone deposition amounts accumulated over the one-month period (g hectare^{-1}). All values but the dry deposition amounts are averaged for each grid cell over the one-month period.

4.4. Association with coastal winds

In order to understand impacts of the enhanced ozone deposition velocities over the ocean on the changes in the spatio-temporal distributions of ozone deposition and concentration in both the northern Gulf of Mexico and the inland area, additional CMAQ simulations were performed using the same initial and boundary concentration conditions for Case 3 and 2 during the two-day period (1800 CST, 5 – 1800 CST, 7) in August. Especially the Louisiana Gulf Coast region was subject to the low average wind speeds over the sea and the marked sea-breeze circulation in the Texas Gulf coast area. These wind conditions help us to identify the chemical effects of iodide and provide us an insight on how on- and off-shore ozone deposition and concentration are affected by this process.

Fig. 5 shows spatial features of differences in the modeled ozone dry deposition velocities, dry deposition amounts and ambient concentrations between Case 2 and 3 at selected times during the period. The differences in deposition amounts between two cases began to appear over the sea in the early morning of 6 August and then were noticeable after noon. At 1200 and 1800 CST, significant differences were found along the northeastern Texas Gulf coast to Louisiana coast with somewhat different patterns compared to that of dry deposition velocity, caused by the combined effects of the enhanced ozone removals by chemical reactions with the dissolved iodide under low winds and the increased ambient ozone concentrations over the offshore region during daytime. The negative differences were also founded inland near the coast as the sea-breeze wind penetrated inland at 1800 CST 6 August, which spread out further inland at 0000 and 0600 CST 7 August. As noted in the previous section, this is caused by the advection of the air with relatively low ozone concentrations due to the enhanced deposition onto the seawater.

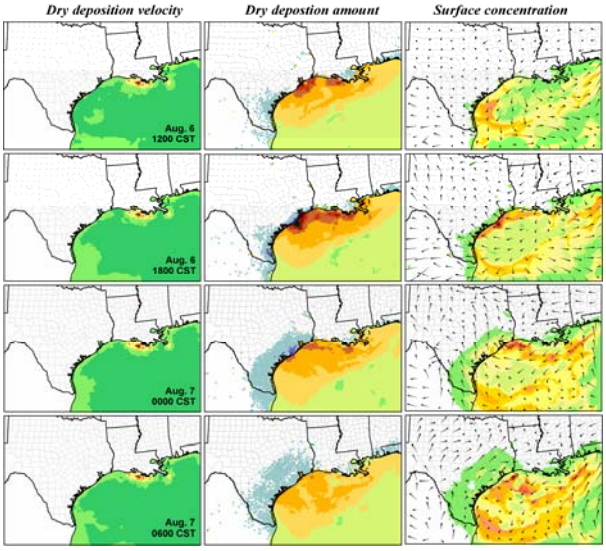

Fig. 5. Differences (Case 3 minus Case 2) in dry deposition velocities (cm s^{-1}), dry deposition amounts (g hectare $^{-1}$) and surface concentrations of ozone simulated at 1200 and 1800 CST August 6 and 0000 and 0600 CST August 7. The wind-vector length is proportional to wind speed ranging from 0 to 10 m s^{-1}. Numbers in the legend box indicate the lower values for given classes.

On the other hand, the pattern of the difference in ambient ozone concentration does not exactly correspond to those of deposition amount because of the advection effects by onshore winds. However, the area with the relatively large differences in both deposition amounts and concentrations at 1800 CST are similar to each other, implying that ozone loss by dry deposition plays an important role in changing ambient concentrations over the sea. The maximum concentration difference (about 2.5 ppb) resulting from the iodide effect was founded over the Brazoria-Galveston offshore at 1800 CST. With the penetration of marine air by the sea-breeze, small but noticeable changes in ozone concentration occurred inland near the coast (0000 CST 7 August). The small difference over the land is partly due to the mitigating effects of horizontal and vertical mixing processes. The variations in ozone concentration and wind in Fig. 5 indicate the enhanced dry deposition velocity over a seawater surface can even affect ozone concentrations in the coastal and inland area.

5. SUMMARY AND CONCLUSION

In order to estimate the effects of the dissolved iodide on ozone deposition onto the seawater surface, an attempt is made to apply a deposition formulation that takes into account for the reaction of iodide with ozone in the sea micro sublayer (Chang et al., 2004) to the M3DDEP module in CAMQ. We performed one-month CMAQ model simulations incorporating iodide concentrations estimated from satellite measurements over the Gulf of Mexico. The results showed that ozone dry deposition velocities from the modified CMAQ increased markedly over the Gulf of Mexico, especially over the Gulf coast region in Louisiana corresponding to the area with high iodide concentrations. One-month average statistics from a 12-km nested domain indicate that about 70 % enhancement of ozone dry deposition velocity over the coastal sea is attributed to the iodide effect alone, clearly indicating significance of ozone loss due to iodide in the sea surface microsublayer. This confirms the dominant role of the dissolved iodide in ozone reduction onto the sweater pointed out by Garland et al. (1980), Lugo-Fernandez and Roscigno (1999), and Chang et al. (2004).

An in-depth analysis of 6-7 August showed pronounced effects of iodide reaction for the calm wind conditions with the maximum decrease of ozone about 2.5 ppb found over the offshore area of the Brazoria-Galveston in the afternoon. In particular, small but noticeable changes in ozone concentrations over the inland near the coast were seen during the time of inland penetration of the sea-breeze. This shows that enhanced ozone dry deposition velocity due to the iodide reaction in the sea-surface microsublayer can lead to a significant difference in the ozone deposition flux in the coastal area which experience high ozone concentrations associated with industrial activities and land-sea circulation.

Acknowledgements

This work was funded by the Minerals Management Service (MMS) and its contributions are acknowledged.

6. REFERENCES

Aldaz, L., 1969: Flux measurements of atmospheric ozone over land and water. *J. Geophys. Res.,* 74, 6943-6946.

Chang, Wonil, G. Brian, Lee, M., 2004: Ozone deposition to the sea surface: chemical enhancement and wind speed dependence, *Atmos. Environ*., 38, 1053–1059.

Galbally, I.E. Roy, C.R., 1980: Destruction of ozone at the earth's surface. *Q. J. Roy. Meteor. Soc.,* 106, 599–620.

Gallagher, M.W., Beswick, K.M., Coe, H., 2001: Ozone deposition to coastal water. *Q. J. Roy. Meteor. Soc.,* 127, 539–558.

Garland, J.A., Elzerman, A.W., Penkett, S.A., 1980: The mechanism for dry deposition of ozone to seawater surface. *J. Geophys. Res.,* 85, 7488–7492.

Kawa, S.R., Rearson, R., 1989. ozone budgets from the dynamics and chemistry of marine stratocumulus experiment. *J. Geophys. Res.,* 94, 9809-9817.

Lenschow, D., Pearson, R., Stankov, B., 1982: Measurements of ozone vertical flux to ocean and forest. *J. Geophys. Res.,* 87, 8833–8837.

Liss, P., Merlivat, L., 1986: Air–gas exchange rate: introduction and synthesis. In:Buat-Menard, P. (Ed.), The Role of Air–Sea Exchange in Geochemical Cycling. D. Reidel, Hingham, MA, pp. 113–129.

Lugo-Fernandez, A., Roscigno, P.F., 1999: Environmental assessment of the impact of ozone to the neuston of the sea surface microlayer of the Gulf of Mexico. Environ. *Monit. Assess.,* 55, 319–346.

Rabalais, N. N., Smith, L. E., Overton, E. B., Zoeller, A. L.: 1993, Influence of Hypoxia on the Interpretation of Effects of Petroleum Production Activities, U.S. Department of the Interior, Minerals Management Service, Gulf of Mexico OCS Region, OCS Study MMS 930022. New Orleans, LA

Riemer, D.D., Milne, P.J., Zika, R.G., Pos, W.H., 2000. Photoproduction of nonmethane hydrocarbons (NMHCs) in seawater. *Mar. Chem.,* 71, 177–198.

Slinn, W.G.L., Hasse, L., Hicks, B.B., Hogan, A.W., Lal, D., Liss, P.S., Munnich, K.O., Sehmel, G.A., Vittori, O., 1978. Review paper: Some aspects of transfer of atmosphere trace constituents past the air-sea interface. *Atmos. Environ.,* 12, 2055-2087.

TCEQ, 2004: Revisions to the State Implementation Plan (SIP) for the Control of Ozone Air Pollution: Houston/Galveston/ Brazoria Ozone Nonattainment Area, Report, Texas Commission On Environmental Quality, P.O. Box 13087, Austin, Texas 78711-3087.

Wanninkhof, R., 1992: Relationship between wind speed and gas exchange over the ocean. *J. Geophys. Res.,* 97, 7373-7382.

Wong, G.T.E., Zhang, L., 1992: Changes in iodine speciation across coastal hydrographic fronts in southern United States continental shelf water. *Cont. Shelf Res.,* 12 (5/6), 717-733.